Article:
Georgiou, K., McGhee, K.E., Jayaprakash, R. orcid.org/0000-0002-2021-1601 et al. (1 more author) (2021) Observation of photon-mode decoupling in a strongly coupled multimode microcavity. The Journal of Chemical Physics, 154 (12). 124309. ISSN 0021-9606

https://doi.org/10.1063/5.0038086

The Journal of Chemical Physics

Observation of photon-mode decoupling in a strongly coupled multimode microcavity

Cite as: J. Chem. Phys. **154**, 124309 (2021); https://doi.org/10.1063/5.0038086
Submitted: 18 November 2020 • Accepted: 08 March 2021 • Published Online: 24 March 2021

Kyriacos Georgiou, Kirsty E. McGhee, Rahul Jayaprakash, et al.

The Journal of Chemical Physics ARTICLE scitation.org/journal/jcp

Observation of photon-mode decoupling in a strongly coupled multimode microcavity

Cite as: J. Chem. Phys. 154, 124309 (2021); doi: 10.1063/5.0038086
Submitted: 18 November 2020 • Accepted: 8 March 2021 •
Published Online: 24 March 2021

Kyriacos Georgiou,[1,2,a)] Kirsty E. McGhee,[1] Rahul Jayaprakash,[1] and David G. Lidzey[1,a)]

AFFILIATIONS

[1] Department of Physics and Astronomy, University of Sheffield, Hicks Building, Hounsfield Road, Sheffield S3 7RH, United Kingdom
[2] Department of Physics, University of Cyprus, P.O. Box 20537, Nicosia 1678, Cyprus

Note: This paper is part of the JCP Special Topic on Polariton Chemistry: Molecules in Cavities and Plasmonic Media.
[a)] **Authors to whom correspondence should be addressed:** georgiou.kyriacos@ucy.ac.cy and d.g.lidzey@sheffield.ac.uk

ABSTRACT

We have fabricated organic semiconductor microcavities having an extended optical path-length (up to 2 μm) that contain J-aggregates of a cyanine dye. These structures are studied using optical-reflectivity and are found to be characterized by a series of polaritonic modes. By changing the effective oscillator strength of the dye within the cavity, we evidence a transition from "normal" strong coupling in which the photon modes are coupled to one another via the excitonic transition of the molecular dye to a state in which photon-modes become decoupled. We use an eight-level modified Hamiltonian to describe the optical properties of the system and compare the distribution of the confined optical field in coupled and decoupled structures.

INTRODUCTION

Cavity-polaritons are quasiparticles that are formed when the excitations of a material strongly couple to the photonic field confined by a microcavity.[1] In order to meet the strong coupling condition and enter the so called "strong coupling regime," the interaction potential between light and matter must be greater than the excitation dephasing rate and the rate at which photons escape the cavity.[2] In this regime, the polariton states formed are a linear superposition between photons and the excitations of the material, with the polaritons described as being half-light/half-matter quasiparticles. The first demonstration of polaritons in a microcavity was made using a series of inorganic semiconductor quantum wells at cryogenic temperatures.[3] Soon after, similar effects were explored in an organic semiconductor microcavity, with Rabi-splittings above 100 meV observed at room temperature due to the large oscillator strength and high binding energy of Frenkel excitons.[4]

Cavity-polaritons are bi-dimensional quasiparticles that can be described by their energy and in-plane momentum. In the past decade, organic-exciton polaritons have been used to study and understand a range of effects such as polariton condensation, superfluidity, band-structure formation in polariton lattices, and all-optical polariton logic gates.[5–13] Microcavities containing two different organic semiconductors have also been shown to be characterized by a three-way hybridization, resulting in the formation of "middle" polariton branches.[14] Here, such "middle" branch polaritons have been shown to act as intermediate states that facilitate long-range energy transfer between spatially separated donor–acceptor species.[15–18] Recent work has also shown that strong interactions between an IR electromagnetic field and a vibrational mode of a molecular material can alter molecular potential energy surfaces and affect the rate at which organic materials undergo chemical reactions.[19–23] Here, the ability to accelerate or retard a chemical reaction is expected to have potentially profound applications in synthetic chemistry and bio-optical engineering.

Polariton phenomena are most often studied in structures in which a single photonic mode couples to one or more electronic or vibronic transitions. However, strong coupling and polariton condensation have also been reported in "thick" cavities that support N closely spaced photonic modes that are in resonance with an excitonic species.[24–26] In such studies, the resultant polariton modes have been described using an $(N + 1) \times (N + 1)$ multilevel coupled oscillator model that describes the mutual hybridization of the

photonic modes due to their coupling to the same excitonic transition. This photonic coupling results in the appearance of a series of polariton branches that energetically cross the excitonic resonance, indicating the exciton-mediated coupling of consecutive optical modes. A previous theoretical study has suggested that modeling of multilevel systems should use a different approach from that used to describe a single optical mode that couples to an excitonic transition.[27] This idea has been further developed by Balasubrahmaniyam *et al.*[28] who have shown that when an excitonic resonance with a sufficiently large oscillator strength is placed in a multimode cavity, the polariton modes formed can no longer be described by a conventional $(N + 1) \times (N + 1)$ coupled oscillator model, but a new $(2N) \times (2N)$ Hamiltonian system should be used instead, which treats the photonic modes individually.[28] Here, they suggest that new transitions should emerge as a result of the competition between the finite propagation velocity of light and the lifetime of the strongly coupled emitters inside the cavity.[28]

In this paper, we experimentally demonstrate a transition into this new regime by fabricating thick, multimode cavities containing a strongly coupled J-aggregated organic semiconductor. Structures having extended optical pathlengths similar to those that we describe here are becoming of increasing interest in the field of solution-based polariton chemistry,[22,29,30] and thus, it is important to develop appropriate models to accurately describe their optical properties. We show that by systematically increasing the effective oscillator strength of the organic dye layer within the cavity (while keeping its thickness fixed), we observe a transition into a regime where the photon modes become decoupled and the polariton modes that cross the exciton energy disappear. We use a transfer matrix (TM) model to describe the polariton states formed and show that once photon mode decoupling occurs, a $(2N) \times (2N)$ coupled oscillator model[27,28] can accurately describe the energetic dispersion of the polariton states. Finally, we calculate the electric field distribution in cavities under the two different strong coupling regimes using a TM model and demonstrate that the coupling and decoupling of the photon modes can be evidenced through a change in the distribution of electromagnetic field in the cavity.

RESULTS

The organic-semiconductor used in this study is the fluorescent cyanine dye 5,6-dichloro-2-[[5,6-dichloro-1-ethyl-3-(4-sulfobutyl)-benzimidazol-2-ylidene]-propenyl]-1-ethyl-3-(4-sulfobutyl)-benzimidazolium hydroxide, sodium salt, and inner salt (TDBC). When TDBC molecules are dissolved in a polar solvent, they undergo self-organization to form J-aggregates.[31] Molecular J-aggregates have been extensively used in microcavity research due to their relatively narrow absorption linewidth, superradiant emission, and high oscillator strength that render them suitable systems for strong coupling.[32–36] Here, the TDBC molecules were dissolved in a gelatine/water solution at a range of concentrations by weight. Thin films were then spin-coated from solution, and upon drying, the film contained TDBC J-aggregates.

Figure 1 shows the extinction coefficient of spin-cast TDBC/gelatine films on quartz-coated glass substrates that were created by dissolving TDBC in a gelatine/water blend at different concentrations (between 1% and 6%) by weight. Here, it can be seen that the extinction coefficient increases as the local concentration

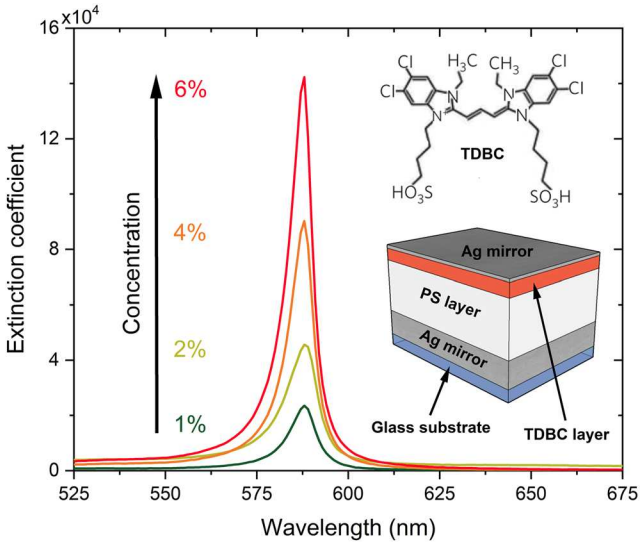

FIG. 1. Extinction coefficient of TDBC films spin-coated from a gelatine/water solution. Here, the films contained concentrations of TDBC in gelatine by weight between 1% (green) and 6% (red). The inset shows the molecular structure of TDBC (top) and a schematic of the optical microcavities used (bottom). The microcavities were fabricated on a glass substrate and consisted of a PS inert spacer-layer and a TDBC active layer positioned between two Ag mirrors.

of TDBC molecules is increased. In the inset of Fig. 1, we show a typical schematic of the microcavity structures explored, along with the molecular structure of TDBC. To fabricate a microcavity, a bottom silver (Ag) mirror with a thickness of 200 nm was first deposited by thermal evaporation onto a quartz-coated glass substrate. Following this, a 1770 nm thick polystyrene (PS) spacer layer was then deposited on top of the Ag mirror, followed by a 320 nm thick TDBC/gelatine film. Here, the two organic layers were spin-coated from different solvents, namely, toluene (PS) and de-ionized (DI) water (TDBC). This allowed stable, well-defined PS and TDBC/gelatine layers to be constructed as these materials had orthogonal solubility in the two casting solvents. Finally, the microcavity structure was completed by the thermal evaporation of a 34 nm thick semi-transparent Ag mirror.

We have fabricated a series of microcavities in which the overall thickness of the cavity layer was kept fixed at 2090 nm. Here, the PS spacer had a thickness of 1770 nm with the TDBC/gelatine layer being 320 nm. In this series of experiments, we systematically increased the concentration of the TDBC dye in the gelatine matrix. To confirm that such structures enter the strong coupling regime, angle-dependent white light reflectivity measurements were performed using a goniometer. The results are summarized in Figs. 2(a), 2(b), 3(a), and 3(b), where we plot 2D reflectivity maps over the angular range of 10°–65° for cavities in which the concentration of the TDBC in gelatine was set to 1%, 2%, 4%, and 6% by weight. We have also used a TM model to calculate the reflectivity of such structures over the same angular range. The results of our simulations are shown in Figs. 2(c), 2(d), 3(c), and 3(d), where it can be seen that the model provides an excellent qualitative description of the experimental results. Here, the experimental 2D plots, shown in Figs. 2(a),

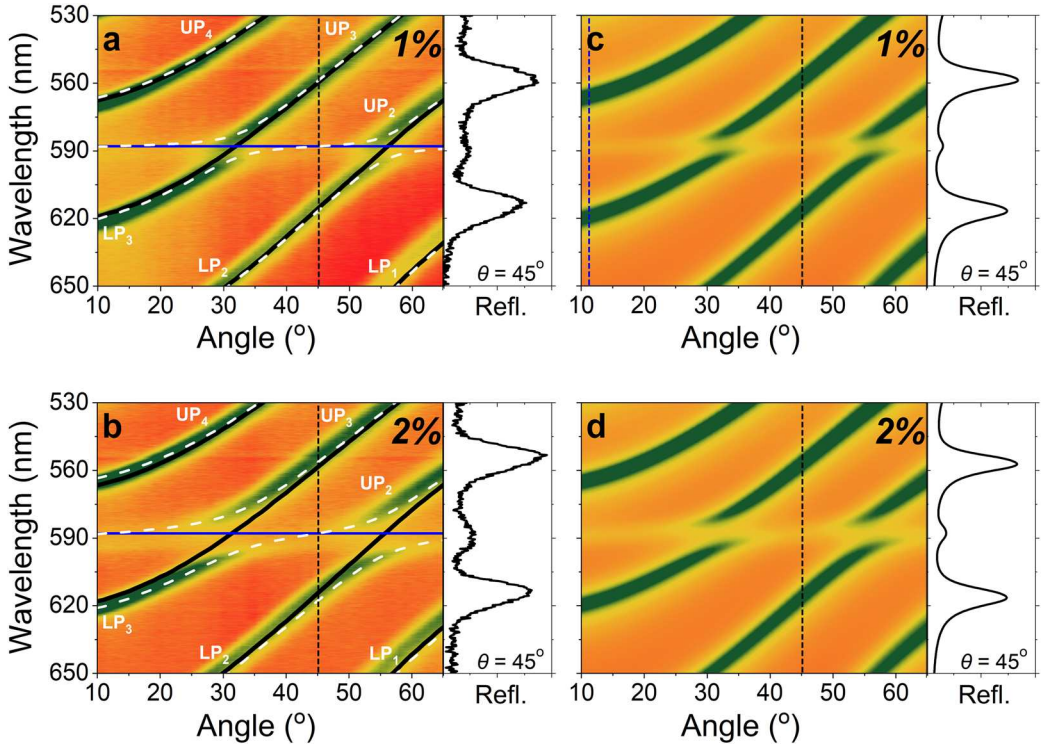

FIG. 2. (a) and (b) Experimental angle-resolved white light reflectivity maps of cavities containing TDBC having a concentration of (a) 1%, and (b) 2% by weight in a gelatine matrix. The reflectivity data were fitted using a conventional $(N + 1) \times (N + 1)$ coupled oscillator model. The blue solid line corresponds to the peak wavelength of the TDBC absorption, the black solid lines show the uncoupled cavity modes extracted by a TM model, and the white dashed lines represent the formed polariton modes. (c) and (d) Simulated reflectivity data using a TM model for cavities containing a layer of (c) 1% and (d) 2% of TDBC in gelatine by weight. The right-hand side panels in (a)–(d) show cross sections of the 2D reflectivity map taken at an angle of 45°, which is marked with black vertical dashed lines in the 2D maps. The blue vertical dashed line in (c) marks the angle of 11°.

2(b), 3(a), and 3(b), are overlaid with the dispersion of the uncoupled photon modes extracted from the TM model (black solid lines) and the peak wavelength of the TDBC absorption (blue solid line). It can be seen that the various modes appear to undergo an anticrossing around the energy of the TDBC exciton qualitatively, and thus, we conclude that the system operates in the strong coupling regime. We justify this conclusion using the optical models that we present below.

The reflectivity data shown in Figs. 2(a) and 2(b) correspond to cavities that contained a TDBC layer having a concentration of 1% and 2% by weight in gelatine, respectively. Here, we fit the dispersion of the various polaritonic states in these two cavities using a "conventional" $(N + 1) \times (N + 1)$ coupled oscillator model as described by

$$E_{N+1} = \begin{bmatrix} E_{TDBC} & g^{(1)}_{TDBC} & g^{(2)}_{TDBC} & g^{(3)}_{TDBC} & g^{(4)}_{TDBC} \\ g^{(1)}_{TDBC} & E^{(1)}_{ph} & 0 & 0 & 0 \\ g^{(2)}_{TDBC} & 0 & E^{(2)}_{ph} & 0 & 0 \\ g^{(3)}_{TDBC} & 0 & 0 & E^{(3)}_{ph} & 0 \\ g^{(4)}_{TDBC} & 0 & 0 & 0 & E^{(4)}_{ph} \end{bmatrix}_{(N+1)\times(N+1)}. \quad (1)$$

In this model, it is assumed that $N = 4$ photon modes hybridize simultaneously with the TDBC excitons, resulting in an exciton-mediated coupling that mixes photon and exciton modes. Here, E_{TDBC} is the peak energy of the TDBC excitons, E_{ph} represents the energy of the uncoupled photon modes, and g_{TDBC} is the interaction energy between each uncoupled photon mode and the TDBC excitons. The best fit to the data is overlaid in Figs. 2(a) and 2(b) using white dashed lines. We again identify the states evident as being polaritons and label them as lower (LP_n) and upper (UP_n) branch states, where $n = 1, 2, 3, 4$. From the best fit to our model, we determine a Rabi splitting energy between polariton branch pairs LP_2–UP_2 and LP_3–UP_3 of 38 meV in a cavity containing 1% TDBC in gelatine. For the cavity containing 2% TDBC in gelatine, a larger Rabi splitting energy of 66 meV was determined between mode pairs LP_2–UP_2 and LP_3–UP_3. Note that we have previously shown that the Rabi splitting energy in "thick" multimode Fabry–Pérot resonators that consisted of an inert/active bilayer can be slightly different for optical modes of different orders.[37] This effect results from a different degree of overlap between the confined-optical field of the various optical modes and the active layer.[37] However, this effect is negligible in the structures explored here, and we assume a similar interaction energy between the exciton and the various optical modes in each of the different Hamiltonian models.

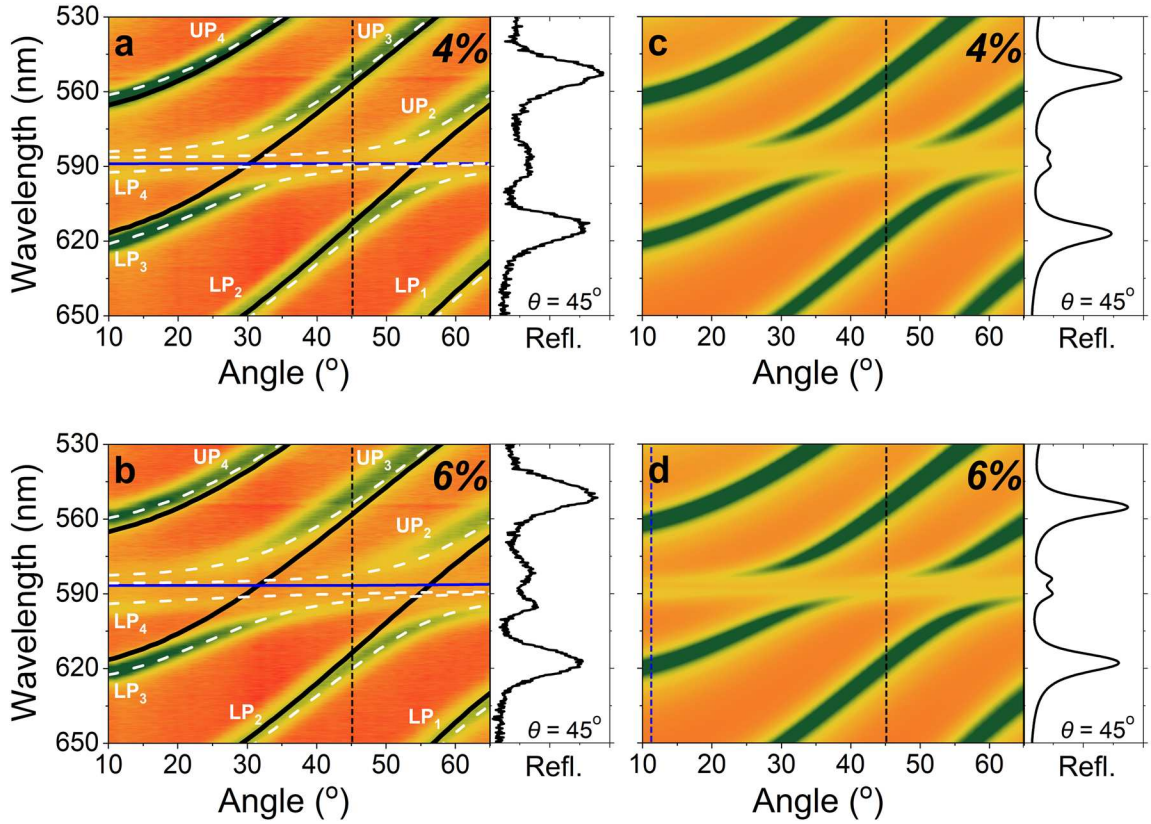

FIG. 3. (a) and (b) Experimental angle-resolved white light reflectivity maps of cavities containing TDBC having a concentration of (a) 4% and (b) 6% by weight in a gelatine matrix. The reflectivity data were fitted using a $(2N) \times (2N)$ coupled oscillator model. The blue solid line corresponds to the peak wavelength of the TDBC absorption, the black solid lines show the uncoupled cavity modes extracted by a TM model, and the white dashed lines represent the polariton modes formed. (c) and (d) Simulated reflectivity data using a TM model for cavities containing a layer of (c) 4% and (d) 6% of TDBC in gelatine by weight. The right-hand side panels in (a)–(d) show cross sections of the 2D reflectivity map at an angle of 45°, which is marked with black vertical dashed lines in 2D maps. The blue vertical dashed line in (d) marks the angle of 11°.

To confirm that our structures operate in the strong coupling regime, we have used the following inequality from the work of Savona *et al.*:[2]

$$g^2 > (\gamma_c^2 + \gamma_x^2)/2, \tag{2}$$

where γ_c and γ_x are the photon and exciton linewidths [half-width at half-maximum (HWHM)] respectively. In Table I, we tabulate the peak energy E_{TDBC} of TDBC excitons, the photon–exciton interaction energy g_{TDBC}, the Rabi splitting energy $\hbar\Omega_{Rabi}^{TDBC}$, and the photon and exciton HWHM linewidths for all cavities used in this study. It can be seen that the condition for strong coupling is met for all four TDBC concentrations. For completeness, we also plot the Rabi splitting energy extracted from our models against the square root of the extinction coefficient for each cavity in Fig. S1 of the supplementary material, demonstrating an expected linear dependence.[4]

We find experimentally (and confirm with our model) that polariton modes LP_3 and UP_2 cross the exciton energy and merge at an angle of 45° creating a mixed LP_3/UP_2 polariton state that is detected via a single dip in the reflectivity spectra [see the right-hand side panels shown in Figs. 2(a)–2(d)]. We focus on the region around which the mixed polariton mode LP_3/UP_2 crosses the exciton energy, as it is at this point where we expect to see maximum interaction (coupling) between adjacent photonic modes. Here, the mixing between different photon modes and TDBC excitons in

TABLE I. Peak energy (E_{TDBC}) of TDBC excitons, photon–exciton interaction energy (g_{TDBC}), Rabi splitting energy ($\hbar\Omega_{Rabi}^{TDBC}$), HWHM linewidth of photon mode (γ_c), and TDBC absorption (γ_{TDBC}) for cavities containing 1%, 2%, 4%, and 6% TDBC in gelatine by weight.

Cavity (%)	E_{TDBC} (eV)	g_{TDBC} (meV)	$\hbar\Omega_{Rabi}^{TDBC}$ (meV)	γ_x^{TDBC} (meV)	γ_c (meV)
1	2.11	19	38	12.5	13.5
2	2.11	33	66	12.5	13.5
4	2.11	40	80	10.5	13.5
6	2.11	48	96	8.5	13.5

the LP_3/UP_2 branch is confirmed by their Hopfield coefficients, which are obtained from Eq. (1) and plotted in Fig. S2(a) of the supplementary material. As shown in Fig. S2(a) of the supplementary material, this polariton branch mostly consists of photon mode $N + 1$ at small angles and photon mode N at large angles. At the point at which the polariton mode crosses the exciton energy around 45° [black dashed vertical lines in Figs. 2(a) and 2(b) and Fig. S2(a) of the supplementary material], the mixing between the two photon modes is maximized. As we show later, we can determine the mode number (N) of the various photon-modes that couple into the LP_3/UP_2 branch by modeling the distribution of the electric field within the cavity. Previously, the crossing of polariton and exciton modes has been attributed to an adiabatic transformation of polariton states from higher to lower order cavity modes due to the fact that the photon modes are hybridized through their mutual coupling to excitons.[28] The data shown in Figs. 2(a)–2(d) and Fig. S2(a), therefore, confirm that these cavities operate within the photon-coupled regime, a regime where all polariton states contain contributions from TDBC excitons and various photonic modes.

We now turn our attention to the angle-resolved white light reflectivity plots shown in Figs. 3(a) and 3(b) that correspond to cavities that contain TDBC molecules in gelatine at a concentration of 4% and 6% by weight, respectively. We again use a TM model to describe the measured reflectivity spectra, as shown in Figs. 3(c) and 3(d). From this, we can determine the energy of the uncoupled photon modes and the peak energy of the TDBC absorption, which we plot in Figs. 3(a) and 3(b) using black and blue solid lines, respectively. Again, we label the various upper and lower polariton branches UP_n and LP_n, where $n = 1, 2, 3, 4$. As it can be seen from reflectivity maps of both cavities, there is a polariton mode anticrossing between branches LP_2–UP_2 and LP_3–UP_3 at photon–exciton resonance angles of 30° and 55°. Notably, we also detect an anticrossing between polariton branches LP_3 and UP_2 at an angle of 45°. This can be seen in the right-hand side panels of each of Figs. 3(a)–3(d), where two peaks are evident around the exciton energy. This is in contrast to the continuous transition between polariton modes LP_3 and UP_2 represented by a single peak (the mixed polariton states) as seen in Figs. 2(a)–2(d). As we show later, this splitting necessarily results in the formation of polariton modes that are simply composed of a mixture of TDBC excitons and a single photonic mode. Such a splitting between polariton modes has been predicted in a recent theoretical paper by Balasubrahmaniyam *et al.* and assigned to a photon mode decoupling mechanism.[28] Here, it was shown that such photon-decoupling occurs due to the competition between the group velocity of light confined within the cavity and the lifetime of the emitters coupled to the cavity modes. In our structures, we are able to increase the effective oscillator strength and refractive index of a film by increasing the concentration of TDBC molecules, a process that will lead to a reduction in the group velocity of light within the cavity.[28] As we confirm below, this increase in molecular concentration drives a transition from a photon-coupled to a photon-decoupled regime; however, at present, we are currently not able to define the exact TDBC concentration at which this transformation takes place.

To describe the photon-decoupled cavities, we have used a $(2N) \times (2N)$ Hamiltonian coupled oscillator model outlined in the following equation to describe the $2N$ observed polariton branches:

$$E_{2N} = \begin{bmatrix} E_{TDBC}^{(1)} & g_{TDBC}^{(1)} & 0 & 0 & 0 & 0 & 0 & 0 \\ g_{TDBC}^{(1)} & E_{ph}^{(1)} & 0 & 0 & 0 & 0 & 0 & 0 \\ 0 & 0 & E_{TDBC}^{(2)} & g_{TDBC}^{(2)} & 0 & 0 & 0 & 0 \\ 0 & 0 & g_{TDBC}^{(2)} & E_{ph}^{(2)} & 0 & 0 & 0 & 0 \\ 0 & 0 & 0 & 0 & E_{TDBC}^{(3)} & g_{TDBC}^{(3)} & 0 & 0 \\ 0 & 0 & 0 & 0 & g_{TDBC}^{(3)} & E_{ph}^{(3)} & 0 & 0 \\ 0 & 0 & 0 & 0 & 0 & 0 & E_{TDBC}^{(4)} & g_{TDBC}^{(4)} \\ 0 & 0 & 0 & 0 & 0 & 0 & g_{TDBC}^{(4)} & E_{ph}^{(4)} \end{bmatrix}_{(2N)\times(2N)}. \quad (3)$$

Here, E_{TDBC} is again the peak energy of the TDBC excitons, E_{ph} represents the energy of the uncoupled photon modes, and g_{TDBC} is the interaction energy between the uncoupled photon modes and TDBC excitons. This model explicitly assumes that each of the N photon modes couples to the TDBC excitons individually. Diagonalization of Eq. (3) gives the energies of $N = 4$ polariton mode pairs, with each pair of polaritons being associated with a single photon mode. This effect is confirmed by the Hopfield coefficients of polariton mode LP_3 that we plot in Fig. S2(b) of the supplementary material. Here, we can see that LP_3, for example, is simply composed of a mixture of TDBC excitons and a single photonic mode, with no hybridization with other photonic modes predicted.

The results of the best fit of Eq. (3) to the dispersion of the polariton modes are shown using white dashed lines in Figs. 3(a) and 3(b). Using this model, we extract Rabi splitting energies of 80 and 96 meV between the lower and upper polariton modes in cavities containing 4% and 6% TDBC in gelatine, respectively. We have applied the same analysis using the photon and exciton HWHM linewidths and confirm that such cavities operate in the strong coupling regime [see Eq. (2) and data summary in Table I].

To demonstrate the significantly improved description of the cavity dispersion using the photon-decoupled model, we replot the experimental reflectivity maps shown in Figs. 3(a) and 3(b) in Fig. S3 of the supplementary material. Here, data are fit using a $(2N) \times (2N)$ photon-decoupled and a $(N + 1) \times (N + 1)$ photon-coupled Hamiltonian model. This analysis shows that the photon-coupled model does not describe the splitting of polariton modes around the exciton energy, with this effect only really being reproduced accurately by the photon-decoupled model.

To understand the effect of photon mode decoupling in more detail, we have used a TM model to calculate the amplitude of the electric field inside two strongly coupled cavities, one that operates in the photon-coupled regime and the other being photon-decoupled. The results of our model are shown in Figs. 4(a) and 4(b) where we plot color maps of the spatial distribution of the electric field as a function of wavelength for two cavities (1% and 6% TDBC in gelatine) whose modeled angular-dependent reflectivity spectra are shown in Figs. 2(c) and 3(d). Note that for each cavity, the field was calculated at an angle of 11° [as marked using blue vertical dashed lines in Figs. 2(c) and 3(d)]. At this point, polariton modes UP_4 and LP_3 are equally spaced in energy on either side of the exciton energy, and at this particular angle, we expect maximum interaction between the adjacent photon modes.

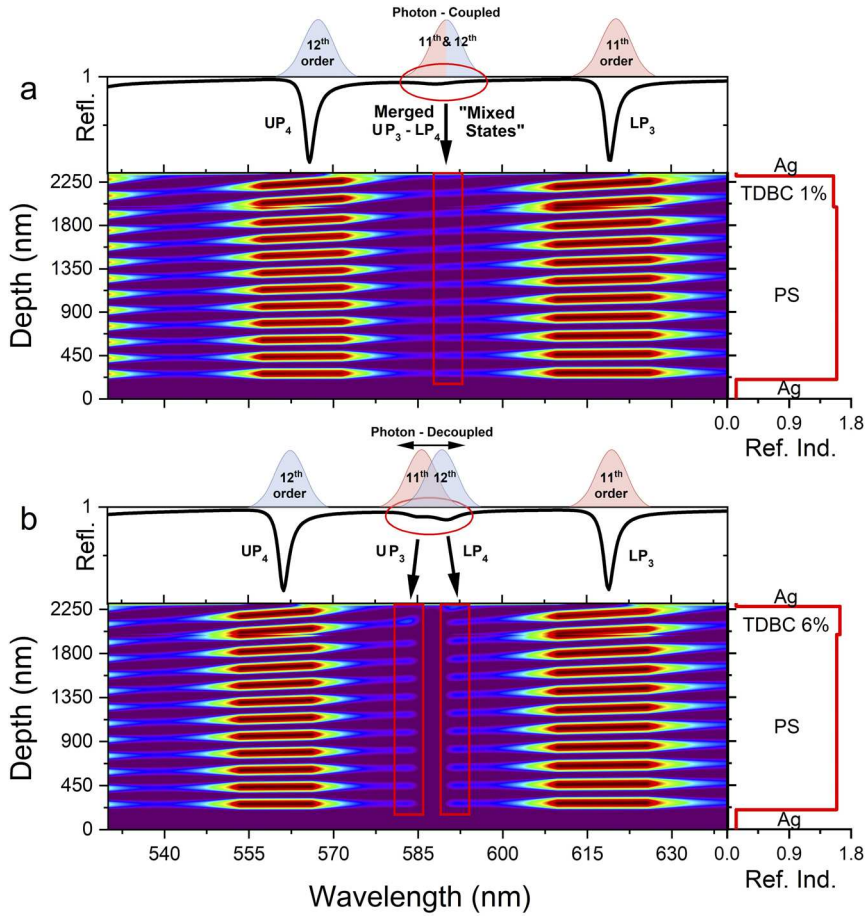

FIG. 4. Simulated 2D plots of the electric field amplitude in (a) a photon-coupled and (b) a photon-decoupled cavity containing 1% and 6% TDBC in gelatine by weight, respectively. The black solid lines plot the modeled TM reflectivity for each cavity at an angle of 11°. The structure is defined using the refractive index of each material as shown with a red solid line in the right-hand side panels.

Figures 4(a) and 4(b) plot the electric field amplitude as a function of wavelength for the cavities containing 1% and 6% TDBC in gelatine by weight, respectively. For completeness, we indicate the different layers within the microcavity structure via their refractive index with this information being plotted in the right-hand side panel. We also plot the refractive index of the various layers of the cavity as a function of wavelength and distance from the substrate in Fig. S4 of the supplementary material. Table S1 of the supplementary material also summarizes the various parameters used in the TM model to describe the distribution of the electric field in the various cavities.

We first consider the cavity containing 1% TDBC by weight [Fig. 4(a)]. As it can be seen, the electric field peaks at wavelengths that correspond to LP_3 and UP_4, with these modes being comprised of 11 and 12 field antinodes, respectively. This indicates that polariton mode LP_3 results from a coupling between an 11th order optical mode with the TDBC excitons, while UP_4 is a mixture between TDBC excitons and a 12th order optical mode as shown by the red and blue shaded areas above reflectivity spectra of Fig. 4(a). Mixed polariton states are located at 588 nm and are marked using a red circle. These modes result from a merging between modes LP_4 and UP_3 [note that, however, mode LP_4 is not marked in Fig. 2(c) as it mainly lies out of the angular measurement range]. The confined electric field at this wavelength is *not* characterized by *either* 11 or 12 antinodes, and thus, we are *not* able to firmly connect this polariton state with one particular optical mode. Rather, the spatial distribution of the field suggests a half-integer number of antinodes (marked with a red rectangle). This behavior has also been predicted and explained in Ref. 28 for a thinner strongly coupled cavity where a merging between polariton modes associated with the second and third order optical modes resulted in an accumulated round-trip phase of 5π.[28] In our structures, such mixed polariton states result from a mixture of TDBC excitons with both the 11th and 12th order optical modes.

In Fig. 4(b), we plot the electric field distribution for a cavity having a TDBC concentration of 6% in gelatine by weight, with the electric field amplitude again calculated at an angle of 11°. As it can be seen from the modeled reflectivity spectra in the top panel, there are polariton modes at 561 nm (UP_4), 585 nm (UP_3), 590 nm (LP_4), and 619 nm (LP_3). Here, mode UP_4 is characterized by 12 antinodes confirming that the polariton mode is formed through the coupling between a 12th order cavity mode and the TDBC excitons. Polariton mode LP_3, however, appears to correspond to TDBC excitons coupling to an 11th order cavity mode. Here, photon mode decoupling

results in an anticrossing of polariton states UP_3 and LP_4 (marked by a red circle) around 588 nm with two new electric field maxima formed that we mark using red rectangles. Here, the number of antinodes in each polariton mode indicates the optical mode to which the TDBC excitons are coupled. Significantly, we observe that the polariton modes UP_3 and LP_4 couple to the 11th and 12th order photon modes, respectively (blue and red shaded areas), as evident by the different number of antinodes formed (11 and 12). This again confirms that the split pair of polariton states that we create (UP_3 and LP_4) are each formed by exciton coupling to different photon modes without any mixing between photonic-states.

In summary, we have shown that as the exciton oscillator strength in an extended "multi-photon mode" cavity is increased, the system can only accurately be described by a photon-decoupled model. We believe that this understanding will be critical for the accurate description of multi-photon cavities that are of significant interest for vibrational strong coupling and solution-based polariton chemistry.[22,29,30] It is interesting to speculate on the possible consequences of such a transition. Clearly, the polaritonic states created in a multi-photon cavity are delocalized throughout the cavity, and thus, much of the phenomenology that occurs in a photon-coupled cavity is likely to apply in a decoupled cavity. Indeed, we have recently confirmed that polariton-assisted energy transfer occurs between molecular dyes over length-scales of up to 2 μm in a photon-decoupled cavity.[38] Such effects may also be important in quantum information processing systems in which different cavity modes are used to create interacting qubits.[39–41]

CONCLUSIONS

We have fabricated a series of multimode optical cavities containing different concentrations of the strongly coupled J-aggregated dye TDBC. Using angle-resolved white-light reflectivity measurements, we determine a transition between two different regimes within the strong coupling regime. This transition was achieved by changing the oscillator strength of the active layer and became evident through either splitting or merging of polariton states associated with the different confined photon modes. In these two regimes, the photon modes either couple to each other via their mutual hybridization with the TDBC excitons or become decoupled from each other. Two coupled oscillator models with different dimensionality are used to describe the dispersion of the polariton modes in the photon-coupled and photon-decoupled regimes, underlying the necessity of using an appropriate Hamiltonian that takes into account such effects. The electric field distribution within the cavity (modeled using a TM model) has been used to show how the different photon modes are mixed into the various polariton states, with this distribution changing substantially when the system transitions from the photon-coupled to decoupled regimes.[28]

METHODS

Organic molecule solutions and films

TDBC (FEW Chemicals GmbH) was dissolved at 1%, 2%, 4%, and 6% by weight in a 70 mg/mL solution of gelatine in DI water. All solutions were heated to 65 °C with films then spin-cast by depositing 100 μL onto quartz-coated glass substrates. Polystyrene (PS: molecular weight ~350 000, Sigma-Aldrich) was added at 100 mg/mL in toluene at 65 °C and stirred until dissolved. This was then allowed to cool at room temperature, with 200 μl being used to spin-coat thin films. A Bruker DektakXT profilometer was used to measure the thickness of all films.

Microcavity fabrication

The bottom mirror of each cavity consisted of 200 nm of Ag, which was evaporated using an Ångstrom Engineering thermal evaporator. A PS layer was spin-coated onto the Ag, followed by a TDBC/gelatine layer. To complete the cavity, a 34 nm thick, semi-transparent Ag mirror was then thermally evaporated onto the TDBC/gelatine layer.

UV–vis absorption and angle-dependent white light reflectivity measurements

UV–vis absorption of the TDBC/gelatine films was measured using a Horiba Fluoromax 4 fluorometer. Angle-dependent white light reflectivity measurements were carried out using a motorized goniometer setup equipped with an excitation arm and a collection arm. A halogen–deuterium white light source (DH-2000-BAL) was coupled with an optic fiber to the excitation arm, with reflected light imaged into an Andor Shamrock SR-303i-A CCD spectrometer coupled to the collection arm.

SUPPLEMENTARY MATERIAL

See the supplementary material for Rabi splitting energy as a function of the square root of the extinction coefficient, Hopfield coefficients in photon-coupled and photon-decoupled microcavities, comparison of photon-coupled and photon-decoupled Hamiltonian models, and the parameters used in the TM model used to calculate the electric field distribution.

AUTHORS' CONTRIBUTIONS

K.G. and K.E.M. contributed equally to this work.

ACKNOWLEDGMENTS

We thank the UK EPSRC for funding this research via the "Hybrid Polaritonics" Program Grant No. EP/M025330/1 and for funding a PhD scholarship for K.E.M. through a DTG allocation. K.G. acknowledges support from the University of Cyprus through the Research Fellowship Program "Onisilos." K.G. conceived the idea. K.G. and K.E.M. fabricated the samples, performed the optical experiments, and analyzed the data. R.J. performed the transfer matrix and coupled oscillator modeling. All authors discussed the results. K.G. and K.E.M. wrote this manuscript with significant contributions from D.G.L. who also oversaw the whole project.

DATA AVAILABILITY

The data that support the findings of this study are available within the article and its supplementary material.

REFERENCES

[1] A. V. Kavokin, J. J. Baumberg, G. Malpuech, and F. P. Laussy, *Microcavities*, 2nd ed. (Oxford University Press, 2007).
[2] V. Savona, L. C. Andreani, P. Schwendimann, and A. Quattropani, Solid State Commun. **93**, 733 (1995).
[3] C. Weisbuch, M. Nishioka, A. Ishikawa, and Y. Arakawa, Phys. Rev. Lett. **69**, 3314 (1992).
[4] D. G. Lidzey, D. D. C. Bradley, M. S. Skolnick, T. Virgili, S. Walker, and D. M. Whittaker, Nature **395**, 53 (1998).
[5] J. D. Plumhof, T. Stöferle, L. Mai, U. Scherf, and R. F. Mahrt, Nat. Mater. **13**, 247 (2014).
[6] K. S. Daskalakis, S. A. Maier, R. Murray, and S. Kéna-Cohen, Nat. Mater. **13**, 271 (2014).
[7] T. Cookson, K. Georgiou, A. Zasedatelev, R. T. Grant, T. Virgili, M. Cavazzini, F. Galeotti, C. Clark, N. G. Berloff, D. G. Lidzey, and P. G. Lagoudakis, Adv. Opt. Mater. **5**, 1700203 (2017).
[8] D. Sannikov, T. Yagafarov, K. Georgiou, A. Zasedatelev, A. Baranikov, L. Gai, Z. Shen, D. Lidzey, and P. Lagoudakis, Adv. Opt. Mater. **7**, 1900163 (2019).
[9] S. K. Rajendran, M. Wei, H. Ohadi, A. Ruseckas, G. A. Turnbull, and I. D. W. Samuel, Adv. Opt. Mater. **7**, 1801791 (2019).
[10] T. Yagafarov, D. Sannikov, A. Zasedatelev, K. Georgiou, A. Baranikov, O. Kyriienko, I. Shelykh, L. Gai, Z. Shen, D. G. Lidzey, and P. G. Lagoudakis, Commun. Phys. **3**, 18 (2020).
[11] G. Lerario, A. Fieramosca, F. Barachati, D. Ballarini, K. S. Daskalakis, L. Dominici, M. De Giorgi, S. A. Maier, G. Gigli, S. Kéna-Cohen, and D. Sanvitto, Nat. Phys. **13**, 837 (2017).
[12] R. Jayaprakash, C. E. Whittaker, K. Georgiou, O. S. Game, K. E. McGhee, D. M. Coles, and D. G. Lidzey, ACS Photonics **7**, 2273 (2020).
[13] A. V. Zasedatelev, A. V. Baranikov, D. Urbonas, F. Scafirimuto, U. Scherf, T. Stöferle, R. F. Mahrt, and P. G. Lagoudakis, Nat. Photonics **13**, 378 (2019).
[14] D. G. Lidzey, D. D. C. Bradley, A. Armitage, S. Walker, and M. S. Skolnick, Science **288**, 1620 (2000).
[15] D. M. Coles, N. Somaschi, P. Michetti, C. Clark, P. G. Lagoudakis, P. G. Savvidis, and D. G. Lidzey, Nat. Mater. **13**, 712 (2014).
[16] X. Zhong, T. Chervy, L. Zhang, A. Thomas, J. George, C. Genet, J. A. Hutchison, and T. W. Ebbesen, Angew. Chem., Int. Ed. **56**, 9034 (2017).
[17] K. Georgiou, P. Michetti, L. Gai, M. Cavazzini, Z. Shen, and D. G. Lidzey, ACS Photonics **5**, 258 (2018).
[18] X. Zhong, T. Chervy, S. Wang, J. George, A. Thomas, J. A. Hutchison, E. Devaux, C. Genet, and T. W. Ebbesen, Angew. Chem., Int. Ed. **55**, 6202 (2016).
[19] J. A. Hutchison, T. Schwartz, C. Genet, E. Devaux, and T. W. Ebbesen, Angew. Chem., Int. Ed. **51**, 1592 (2012).
[20] J. A. Hutchison, A. Liscio, T. Schwartz, A. Canaguier-Durand, C. Genet, V. Palermo, P. Samorì, and T. W. Ebbesen, Adv. Mater. **25**, 2481 (2013).
[21] J. Galego, F. J. Garcia-Vidal, and J. Feist, Nat. Commun. **7**, 13841 (2016).
[22] R. M. A. Vergauwe, A. Thomas, K. Nagarajan, A. Shalabney, J. George, T. Chervy, M. Seidel, E. Devaux, V. Torbeev, and T. W. Ebbesen, Angew. Chem., Int. Ed. **58**, 15324 (2019).
[23] T. W. Ebbesen, Acc. Chem. Res. **49**, 2403 (2016).
[24] D. M. Coles and D. G. Lidzey, Appl. Phys. Lett. **104**, 191108 (2014).
[25] C. P. Dietrich, A. Steude, L. Tropf, M. Schubert, N. M. Kronenberg, K. Ostermann, S. Höfling, and M. C. Gather, Sci. Adv. **2**, e1600666 (2016).
[26] J. Ren, Q. Liao, H. Huang, Y. Li, T. Gao *et al.*, Nano Lett. **20**, 7550 (2020).
[27] S. Richter, T. Michalsky, L. Fricke, C. Sturm, H. Franke, M. Grundmann, and R. Schmidt-Grund, Appl. Phys. Lett. **107**, 231104 (2015).
[28] M. Balasubrahmaniyam, C. Genet, and T. Schwartz, arXiv:2005.03527 (2020).
[29] J. Lather, P. Bhatt, A. Thomas, T. W. Ebbesen, and J. George, Angew. Chem., Int. Ed. **58**, 10635 (2019).
[30] A. Thomas, L. Lethuillier-Karl, K. Nagarajan, R. M. A. Vergauwe, J. George, T. Chervy, A. Shalabney, E. Devaux, C. Genet, J. Moran, and T. W. Ebbesen, Science **363**, 615 (2019).
[31] E. E. Jelley, Nature **138**, 1009 (1936).
[32] T. Virgili, D. Coles, A. M. Adawi, C. Clark, P. Michetti, S. K. Rajendran, D. Brida, D. Polli, G. Cerullo, and D. G. Lidzey, Phys. Rev. B **83**, 245309 (2011).
[33] D. M. Coles, P. Michetti, C. Clark, A. M. Adawi, and D. G. Lidzey, Phys. Rev. B **84**, 205214 (2011).
[34] D. M. Coles, P. Michetti, C. Clark, W. C. Tsoi, A. M. Adawi, J.-S. Kim, and D. G. Lidzey, Adv. Funct. Mater. **21**, 3691 (2011).
[35] P. Michetti and G. C. La Rocca, Phys. Rev. B **77**, 195301 (2008).
[36] P. Michetti and G. C. La Rocca, Phys. Rev. B **79**, 035325 (2009).
[37] K. Georgiou, R. Jayaprakash, and D. G. Lidzey, J. Phys. Chem. Lett. **11**, 9893 (2020).
[38] K. Georgiou, R. Jayaprakash, A. Othonos, and D. G. Lidzey, "Ultralong-range polariton-assisted energy transfer in organic microcavities" (unpublished) (2021).
[39] Y.-L. Dong, X.-B. Zou, S.-L. Zhang, S. Yang, C.-F. Li, and G.-C. Guo, J. Mod. Opt. **56**, 1230 (2009).
[40] F. O. Prado, F. S. Luiz, J. M. Villas-Bôas, A. M. Alcalde, E. I. Duzzioni, and L. Sanz, Phys. Rev. A **84**, 053839 (2011).
[41] A. Wickenbrock, M. Hemmerling, G. R. M. Robb, C. Emary, and F. Renzoni, Phys. Rev. A **87**, 043817 (2013).